Available online at www.sciencedirect.com
SCIENCE DIRECT®
International Journal of Heat and Mass Transfer 47 (2004) 271–286
International Journal of HEAT and MASS TRANSFER
www.elsevier.com/locate/ijhmt

Numerical study on supersonic combustion with cavity-based fuel injection

Kyung Moo Kim [1], Seung Wook Baek *, Cho Young Han [2]

Division of Aerospace Engineering, Department of Mechanical Engineering, Korea Advanced Institute of Science and Technology, 373-1 Kusung-dong, Yusung-ku, Taejon 305-701, South Korea

Received 1 November 2002; received in revised form 7 July 2003

Abstract

The present study describes the numerical investigations concerning the combustion enhancement when a cavity is used for the hydrogen fuel injection through a transverse slot nozzle into a supersonic hot air stream. The cavity is of interest because recirculation flow in cavity would provide a stable flame holding while enhancing the rate of mixing or combustion. Several inclined cavities with various aft wall angle, offset ratio and length are evaluated for reactive flow characteristics. The cavity effect is discussed from a viewpoint of total pressure loss and combustion efficiency. The combustor with cavity is found to enhance mixing and combustion while increasing the pressure loss, compared with the case without cavity. But it is noted that there exists an appropriate length of cavity regarding the combustion efficiency and total pressure loss.

Keywords: Supersonic combustion; Injection; Cavity; Total pressure loss; Combustion efficiency

1. Introduction

In the design of a supersonic combustion ramjet (scramjet) engine a problem of fuel injection as well as flame holding is known to play a very important role. In order to promote its performance, fuel and air must be mixed at the molecular level in the near field of the fuel injection. The strategy often requires the placement of physical obstructions in the combustor to provide streamwise vortices that enhance the mixing of fuel and air. One of the simplest approaches is to use the backward facing step [1]. While generating a recirculation zone behind the step, that contains the hot gases in it, it serves as a continuous ignition source. This approach can provide sustained combustion, but it has a disadvantage of relatively high stagnation pressure loss. In recent years, a cavity flame holder, which is an integrated fuel injection/flame-holding approach, has been proposed as a new concept for flame holding and stabilization in supersonic combustor. It, designed by CIAM (Central Institution of Aviation Motors) in Moscow, was used for the first time in a joint Russian/French dual-mode scramjet flight-test [2]. Experimentally, the use of a cavity after the ramp injector was found to significantly improve the hydrocarbon combustion efficiency in a supersonic flow. Similar flame stabilization method, employed by Ben-Yakar et al. [3] in a solid-fuel supersonic combustor, demonstrated a self-ignition as well as sustained combustion of polymethyl-methacrylate (PMMA) for supersonic flow conditions.

The presence of a cavity on an aerodynamic surface could have a large impact on the flow surrounding it.

* Corresponding author. Tel.: +82-42-869-3714; fax: +82-42-869-3710.

E-mail addresses: pmj6273@hanafos.com (K.M. Kim), swbaek@sorak.kaist.ac.kr (S.W. Baek).

[1] Current address: Agency for Defense Development, Technology R&D Center, 4th Div., 2nd Team, Yusung-ku, P.O. Box 35-5, Taejon 305-600, South Korea.

[2] Current address: Satellite Control System Department, Satellite R&D Division, Korea Aerospace Research Institute, Taejon, South Korea.

0017-9310/$ - see front matter
doi:10.1016/j.ijheatmasstransfer.2003.07.004

Nomenclature

a	speed of sound
c_k	mass fraction of species k
C_p	constant pressure specific heat
C_v	constant volume specific heat
D	cavity depth
D_k	diffusion coefficient of species k
e	internal energy
F	x-direction flux vector
G	y-direction flux vector
h	enthalpy
J	Jacobian
k_{fi}, k_{bi}	reaction rate constants
K	thermal conductivity
L	cavity effective length
M	Mach number
p	pressure
Pr	Prandtl number
q_x, q_y	heat flux
Q	conservative variable
R	right eigenvectors
Re	Reynolds number
R_u	universal gas constant
S	source flux
Sc	Schmidt number
T	temperature
u	x-direction velocity
v	y-direction velocity
W_k	molecular weight
x, y	Cartesian coordinates

Greek symbols

γ	specific heat ratio
ξ, η	computational coordinates
ρ	density
μ	viscosity
τ	shear stress
ω	reaction rate

Superscripts and subscripts

k	k-species
l	laminar
n	time step
ref	reference value
t	turbulent
v	viscous
w	wall value
∞	free stream value

The flowfield inside a cavity is characterized by recirculating flow that increases the residence time of the fluid entering the cavity. Because the drag associated with flow separation is much less over a cavity than for a bluff-body, a cavity inside a combustor makes a stable flame holder with relatively little pressure drop. A rectangular cavity driven by a free shear layer provides a well defined configuration to study the flow separation and reattachment. Basically, there are two types of cavity flow: open or closed [4,5]. Their flow-fields are schematically shown in Fig. 1. The open cavity flow normally occurs for length-to-depth ratio, $L/D < 10$. In

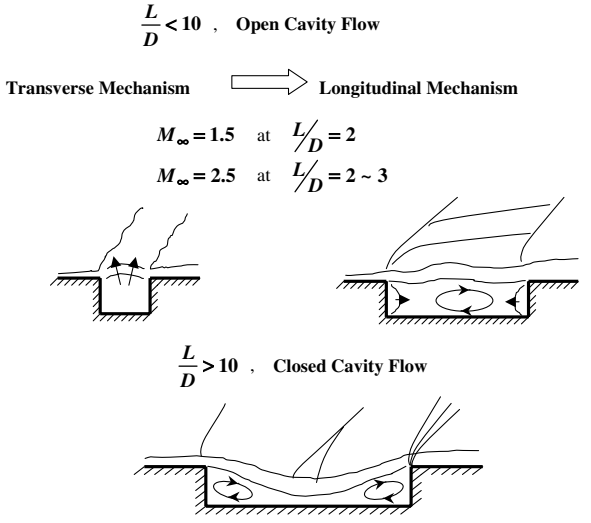

Fig. 1. Various flowfields over cavity for different length to depth ratio, L/D.

this case the shear layer formed at the separation corner spans the entire cavity length and reattaches somewhere along the cavity back face. For $L/D > 10$, the shear layer is unable to span the entire length of the cavity and reattach on the cavity floor, which is the closed cavity flow. Therefore, the closed cavities are characterized by a larger drag coefficient compared with open cavities so that the latter is more desirable in a scramjet combustor. In addition to this operational transition depending on the length-to-depth ratio (L/D), there is another notable feature for cavity flows, which is related to acoustic wave propagation inside the cavity. Researchers suggested that cavity flow oscillations can actually be used to provide enhanced mixing in supersonic shear layers. The mixing was enhanced by the acoustic disturbance and the rate of the enhancement was controlled by cavity shape while the total pressure loss was negligibly small. However before implementing such techniques, one should carefully consider and evaluate any potential thrust loss and noise generation associated with the technique because of this unsteady nature of wave propagation, the flow may become unstable, and unstable combustion in the combustor can be induced. Several control methods have been proposed to suppress the oscillations in cavity. Among others, a cavity with an angled rear wall was devised to suppress the unsteady nature of the free shear layer by eliminating the generation of traveling shocks inside the cavity as shown in Fig. 2 [6]. Otherwise, a small disturbance produced by a mass injector located at upstream of the cavity nearly eliminated the pressure oscillation by altering the shear layers instability characteristics [7]. The numerical studies of cavity-based flameholder have also been done without chemical reaction [8,9]. However, for a practical application to a supersonic combustion, a numerical analysis on the cavity flow for flame holding with chemical reaction is in high demand. Particularly, the numerical analysis of the fuel injection system accompanied by the cavity is rarely studied while it is only recent that its experimental work has been in progress [10,11].

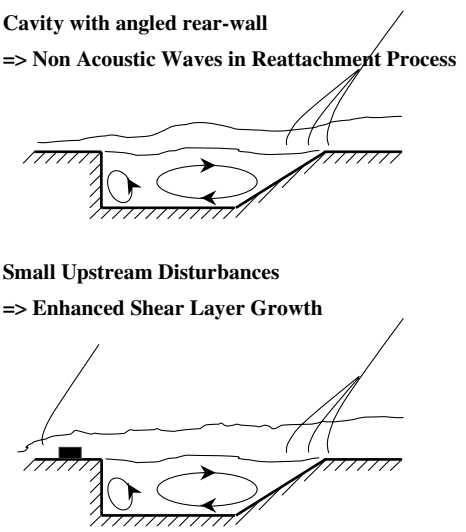

Fig. 2. Flowfields over cavity with an angled rear wall with/without fuel injection.

Based on these facts, the aim of the present study is to investigate the flame holding and combustion enhancement when the inclined cavity is simultaneously used with fuel injection upstream of it. Since a use of the cavity leads to the pressure loss, a counter-balancing effect of the pressure loss and combustion instability should be optimized by exploring various types of cavity configuration under a given condition to find a more effective cavity-based fuel injection system.

2. Numerical formulation

2.1. Governing equations

The governing equations for a general coordinate comprise the mass conservation equation, the full Navier–Stokes equation, energy and species transport equations for a chemically reacting gas composed of N species as follows

$$\frac{\partial \overline{Q}}{\partial t}+\frac{\partial \overline{F}}{\partial \xi}+\frac{\partial \overline{G}}{\partial \eta}=\frac{\partial \overline{F}_{\mathrm{v}}}{\partial \xi}+\frac{\partial \overline{G}_{\mathrm{v}}}{\partial \eta}+\overline{S}, \tag{1}$$

where the conservative vector is $\overline{Q}$ and the convection and viscous terms in the ξ and η direction are $\overline{F}$, $\overline{G}$ and $\overline{F}_{\mathrm{v}}$, $\overline{G}_{\mathrm{v}}$, respectively and defined as below. The source term for chemical reaction is $\overline{S}$.

$$\overline{Q}=\frac{1}{J}Q=\frac{1}{J}\begin{pmatrix}\rho\\ \rho u\\ \rho v\\ \rho e_{\mathrm{t}}\\ \rho_k\end{pmatrix},\quad \overline{S}=\frac{1}{J}S=\frac{1}{J}\begin{pmatrix}0\\ 0\\ 0\\ 0\\ \dot{\omega}_k\end{pmatrix},$$

$$\overline{F}=\frac{1}{J}(\xi_x F+\eta_x G)=\frac{1}{J}\begin{pmatrix}\rho U\\ \rho u U+\xi_x P\\ \rho v U+\xi_y P\\ h\rho U\\ c_k\rho U\end{pmatrix},$$

$$\overline{G}=\frac{1}{J}(\xi_y F+\eta_y G)=\frac{1}{J}\begin{pmatrix}\rho V\\ \rho u V+\eta_x P\\ \rho v V+\eta_y P\\ h\rho V\\ c_k\rho V\end{pmatrix},$$

$$\overline{F}_{\mathrm{v}} = \frac{1}{J}(\xi_x F_{\mathrm{v}} + \eta_x G_{\mathrm{v}}), \quad \overline{G}_{\mathrm{v}} = \frac{1}{J}(\xi_y F_{\mathrm{v}} + \eta_y G_{\mathrm{v}}),$$

$$F_{\mathrm{v}} = \begin{pmatrix} 0 \\ \tau_{xx} \\ \tau_{xy} \\ u\tau_{xx} + v\tau_{xy} - q_x \\ \rho D_k \frac{\partial c_k}{\partial x} \end{pmatrix}, \quad G_{\mathrm{v}} = \begin{pmatrix} 0 \\ \tau_{xy} \\ \tau_{yy} \\ u\tau_{xy} + v\tau_{yy} - q_y \\ \rho D_k \frac{\partial c_k}{\partial y} \end{pmatrix}. \tag{2}$$

The shear stress and heat flux in viscous terms may be denoted by the following equations

$$\tau_{xx} = \frac{\mu}{Re_\infty}\left(\frac{4}{3}\frac{\partial u}{\partial x} - \frac{2}{3}\frac{\partial v}{\partial y}\right), \quad \tau_{yy} = \frac{\mu}{Re_\infty}\left(\frac{4}{3}\frac{\partial v}{\partial y} - \frac{2}{3}\frac{\partial u}{\partial x}\right),$$

$$\tau_{xy} = \frac{\mu}{Re_\infty}\left(\frac{\partial u}{\partial x} + \frac{\partial v}{\partial y}\right),$$

$$q_x = -\frac{1}{Re_\infty Pr(\gamma-1)}K\frac{\partial T}{\partial x} - \frac{1}{Re_\infty Sc_\infty}\rho\sum_{k=1}^{Ns-1} h_k D_k \frac{\partial c_k}{\partial x},$$

$$q_y = -\frac{1}{Re_\infty Pr(\gamma-1)}K\frac{\partial T}{\partial y} - \frac{1}{Re_\infty Sc_\infty}\rho\sum_{k=1}^{Ns-1} h_k D_k \frac{\partial c_k}{\partial y}, \tag{3}$$

where u and v are the velocity components in the x and y directions. Symbols Re_∞, Pr, K, γ, and Sc_∞ are the Reynolds number, Prandtl number, thermal conductivity, specific heat ratio, and Schmidt number, respectively. D_k, h_k, and c_k are diffusion coefficient, enthalpy, and mass fraction for species k.

The transport properties used in this study consist of viscosity, thermal conductivity, and diffusion coefficients, which can be represented by the sum of laminar (molecular) and turbulent components as follows:

$$\mu = \mu_{\mathrm{l}} + \mu_{\mathrm{t}}, \quad K = K_{\mathrm{l}} + K_{\mathrm{t}}, \quad D_k = D_{k\mathrm{l}} + D_{k\mathrm{t}}. \tag{4}$$

The molecular transport properties need to be modeled to account for the effects of temperature and composition. The coefficients thereby introduced have been determined from the Chapmann–Enskog theory that solves the Boltzmann equation with the singled-velocity distribution function [12,13].

The turbulent component for viscosity is calculated using the algebraic eddy viscosity model that is developed by the Baldwin–Lomax [14], whereas those for thermal conductivity and diffusion coefficient are obtained by using the following relations

$$K_{\mathrm{t}} = \frac{C_p \mu_{\mathrm{t}}}{Pr_{\mathrm{t}}}, \quad D_{k\mathrm{t}} = \frac{K_{\mathrm{t}}}{\rho Sc_{\mathrm{t}}} \tag{5}$$

with the turbulent Prandtl number of 0.91 and Schmidt number of 0.9.

For calculation of the specific heat for species k in enthalpy, C_{pk}, a fourth order polynomial equation of temperature is used [15]

$$C_{pk}/R = a_{1,k} + a_{2,k}T + a_{3,k}T^2 + a_{4,k}T^3 + a_{5,k}T^4. \tag{6}$$

Then, the specific heat for mixture at constant pressure is estimated using

$$C_p = \sum_{k=1}^{Ns} c_k C_{pk}. \tag{7}$$

In order to close the system of equations, Eq. (1), the equation of state is also used for calculation of pressure. The macroscopic thermodynamic properties of the gas are related through the general equation of state such that

$$p = p(\rho, e, \rho_k), \quad k = 1, 2, \ldots, N-1. \tag{8}$$

Since the total mass density is known, only $N-1$ species are independent for a chemical system of N species. If the intermolecular forces and the volume occupied by the molecules are negligible, the gas mixture pressure p may be expressed by

$$p = \rho R_{\mathrm{u}} T \sum_{k=1}^{Ns} \frac{c_k}{W_k} = R_{\mathrm{u}} T \sum_{k=1}^{Ns} \frac{\rho_k}{W_k}, \tag{9}$$

where R_{u} and W_k are the universal gas constant and the molecular weight for species k. The mixture enthalpy is denoted by

$$h = \sum_{k=1}^{N} c_k h_k, \quad h_k = h^0_{\mathrm{f}_k} + \int_{T_{\mathrm{ref}}}^{T} C_{pk}\,\mathrm{d}T, \tag{10}$$

where $h^0_{\mathrm{f}_k}$ is the enthalpy of formation and T_{ref} is the reference temperature for thermodynamic properties.

The flux-splitting formulation in the present paper requires a definition of the speed of sound and partial derivatives of p with respect to ρ, e, and c_k which are denoted by p_ρ, p_e, and p_{c_k}. These quantities can be obtained from the equation of state as follows [16]

$$a^2 = \left(\frac{\partial p}{\partial \rho}\right)_s = p_\rho + \frac{p_e p}{\rho^2} + \sum_{k=1}^{N-1}\frac{c_k}{\rho}p_{c_k}, \tag{11}$$

$$p_\rho = \left(\frac{\partial p}{\partial \rho}\right)_{e,\rho_{k,k=1,Ns-1}} = \frac{R_{\mathrm{u}}T}{W_{Ns}} + \frac{\rho R_{\mathrm{u}}}{W}\left(\frac{\partial T}{\partial \rho}\right)_{e,\rho_{k,k=1,Ns-1}}$$
$$= \frac{R_{\mathrm{u}}T}{W_{Ns}} + \frac{R_{\mathrm{u}}}{WC_v}\sum_{k=1}^{Ns-1}\frac{\rho_k}{\rho}(e_k - e_{Ns}), \tag{12}$$

$$p_e = \left(\frac{\partial p}{\partial e}\right)_{\rho,\rho_{k,k=1,Ns-1}} = \frac{\rho R_{\mathrm{u}}}{W}\left(\frac{\partial T}{\partial e}\right)_{\rho,\rho_{k,k=1,Ns-1}} = \frac{\rho R_{\mathrm{u}}}{WC_v}, \tag{13}$$

$$p_{\rho_k} = \left(\frac{\partial p}{\partial \rho_k}\right)_{\rho,e,\rho_{l,l=1,Ns-1,l\neq k}}$$
$$= R_{\mathrm{u}}T\left(\frac{1}{W_k} - \frac{1}{W_{Ns}}\right) + \frac{\rho R_{\mathrm{u}}}{W}\left(\frac{\partial T}{\partial \rho_k}\right)_{\rho,e,\rho_{l,l=1,Ns-1,l\neq k}}$$
$$= R_{\mathrm{u}}T\left(\frac{1}{W_k} - \frac{1}{W_{Ns}}\right) - \frac{R_{\mathrm{u}}}{WC_v}(e_i - e_{Ns}) \tag{14}$$

where

$$W = \frac{1}{\left(\frac{1}{\rho}\right)\sum_{k=1}^{Ns}\left(\frac{\rho_k}{W_k}\right)} \tag{15}$$

is the mean molecular weight for gas mixture. While the constant-volume specific heat of the gas mixture is

$$C_v = \sum \rho_i \frac{C_{pk}}{\rho} - \frac{R_u}{W} \tag{16}$$

the specific internal energy for the kth species is

$$e_k = \int_{T_{ref}}^{T} C_{pk}\,\mathrm{d}T + h_{fk}^0 - \frac{R_u T}{W_k}. \tag{17}$$

2.2. Chemical reaction model

The present finite rate chemistry model includes seven species (H_2, O_2, N_2, H, O, OH, H_2O) and eight elementary reaction steps. The kinetic data for this model are taken from Evans and Schexnayder [17]. The reaction steps and the rate coefficients are given in Table 1. For a set of N_r elementary reactions with Ns species, the model is represented by the following equation

$$\sum_{k=1}^{Ns} \nu'_{i,k} n_k \underset{k_{b,i}}{\overset{k_{f,i}}{\rightleftarrows}} \sum_{k=1}^{Ns} \nu''_{i,k} n_k, \quad i = 1, 2, \ldots, N_r, \tag{18}$$

where, $\nu'_{i,k}$ and $\nu''_{i,k}$ are the stoichiometric coefficients for k species. The forward and backward reaction rate constants are given by the following Arrhenius type of expression

$$\text{Forward reaction:} \quad k_{f,i} = A_{fi} T^{m_{fi}} \exp\left(-\frac{E_{fi}}{R_u T}\right), \tag{19}$$

$$\text{Backward reaction:} \quad k_{b,i} = A_{bi} T^{m_{bi}} \exp\left(-\frac{E_{bi}}{R_u T}\right). \tag{20}$$

The rate of change of mass concentration of species k for reaction step i, then, becomes

$$\dot{\omega}_k = W_k \sum_{i=1}^{N_r} (\nu''_{i,k} - \nu'_{i,k}) \left(k_{f,i} \prod_{l=1}^{Ns} n_l^{\nu'_{i,l}} - k_{b,i} \prod_{l=1}^{Ns} n_l^{\nu''_{i,l}} \right), \quad i = 1, 2, \ldots, N_r. \tag{21}$$

2.3. Numerical treatment

The solution of the governing equations for turbulent supersonic flows requires use of robust as well as accurate scheme. A finite volume approach is used to integrate the governing equations using the Green's theorem and then evaluate the flux at each interface. The convection terms are approximated by the spatially second order Harten–Yee upwind TVD scheme, while the viscous terms are approximated by the second order central difference scheme [18].

Since a large number of species equations is included, the size of blocks in implicit operator becomes so large that the inversion of the implicit operator can be prohibitively expensive without vectorization. As a result, the LU scheme is particularly attractive for non-equilibrium flow. In order to accelerate the computational convergence, the local time stepping approach has also been employed here.

3. Results and discussion

3.1. Code verification

The main objective of this work is to examine the reactive, compressible, viscous, supersonic flow over the cavity when the fuel is injected upstream of it. In order to validate the present numerical method in computing these complex flows, two computing cases are considered here.

As the first case, a problem of injection flow is considered following the experimental configuration and flow conditions for the case of Aso et al. [19].

Table 1
Chemistry model for hydrogen oxidation with air [17]

Reaction	Forward reaction			Backward reaction		
	A_{fk}	m_{fk}	E_{fk}	A_{bk}	m_{bk}	E_{bk}
$H_2 + M \leftrightarrow H + H + M$	5.5×10^{18}	−1.0	51,987	1.8×10^{18}	−1.0	0.0
$O_2 + M \leftrightarrow O + O + M$	7.2×10^{18}	−1.0	59,340	4.0×10^{17}	−1.0	0.0
$H_2O + M \leftrightarrow OH + H + M$	5.2×10^{21}	−1.5	59,386	4.4×10^{20}	−1.5	0.0
$OH + M \leftrightarrow O + H + M$	8.5×10^{18}	−1.0	50,830	7.1×10^{18}	−1.0	0.0
$H_2O + O \leftrightarrow OH + OH$	5.8×10^{13}	0.0	9059	5.3×10^{12}	0.0	503
$H_2O + H \leftrightarrow OH + H_2$	8.4×10^{13}	0.0	10,116	2.0×10^{13}	0.0	2600
$O_2 + H \leftrightarrow OH + O$	2.2×10^{14}	0.0	8455	1.5×10^{13}	0.0	0.0
$H_2 + O \leftrightarrow OH + OH$	7.5×10^{13}	0.0	5586	3.0×10^{13}	0.0	4429

M: third body, $k_{f,i} = A_{fi} T^{m_{fi}} \exp\left(-\frac{E_{fi}}{R_u T}\right)$, $k_{b,i} = A_{bi} T^{m_{bi}} \exp\left(-\frac{E_{bi}}{R_u T}\right)$.

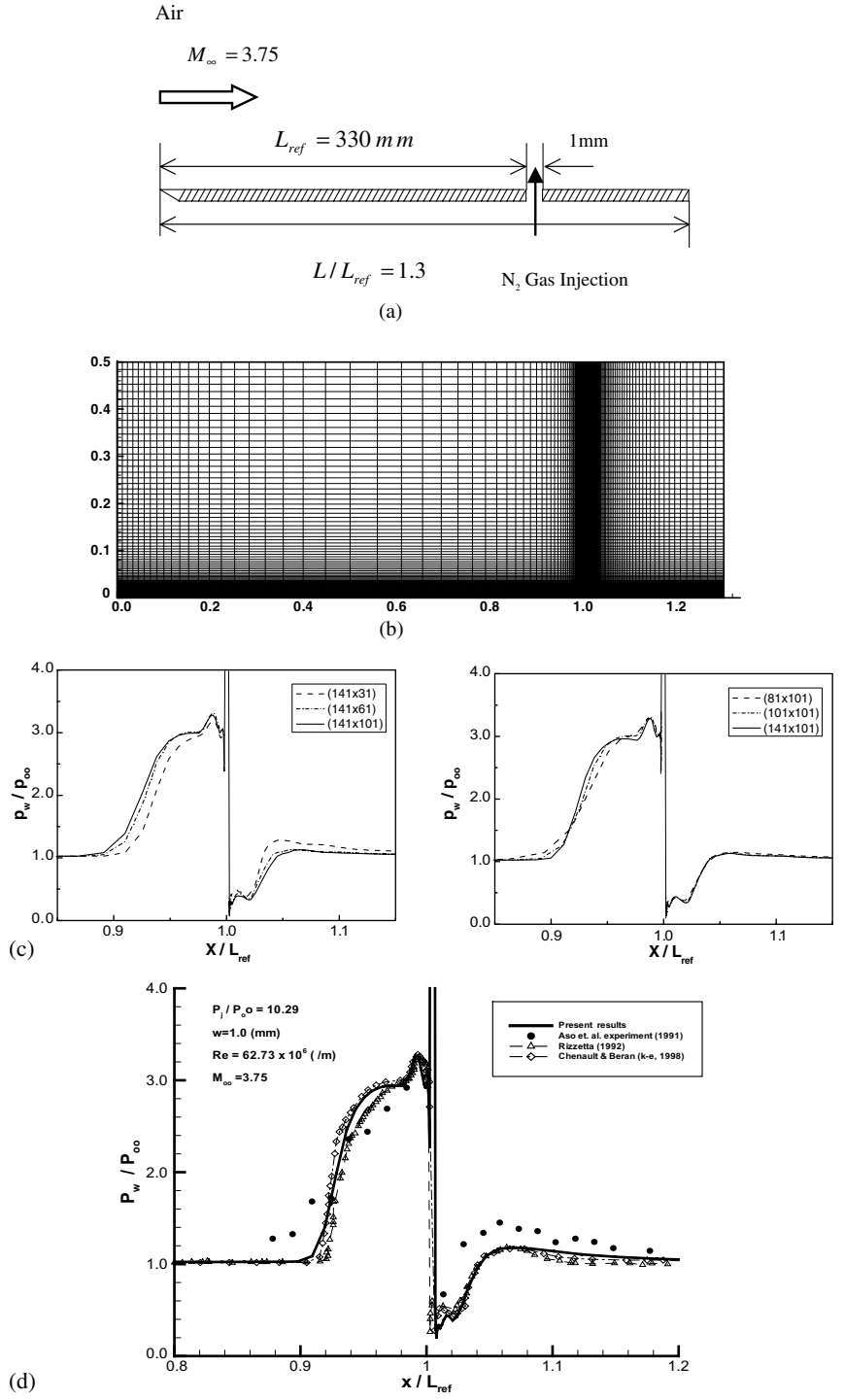

Fig. 3. Wall pressure distribution for the case of injection on the flat plate. (a) Geometry, (b) grid system (141×101), (c) results of grid resolution, (d) wall pressure distribution.

The geometry consists of a flat with a slot as in Fig. 3(a). The distance from the sharp leading edge to the nozzle is $L = 330$ mm, following the experimental configuration. The calculation is conducted for the condi-

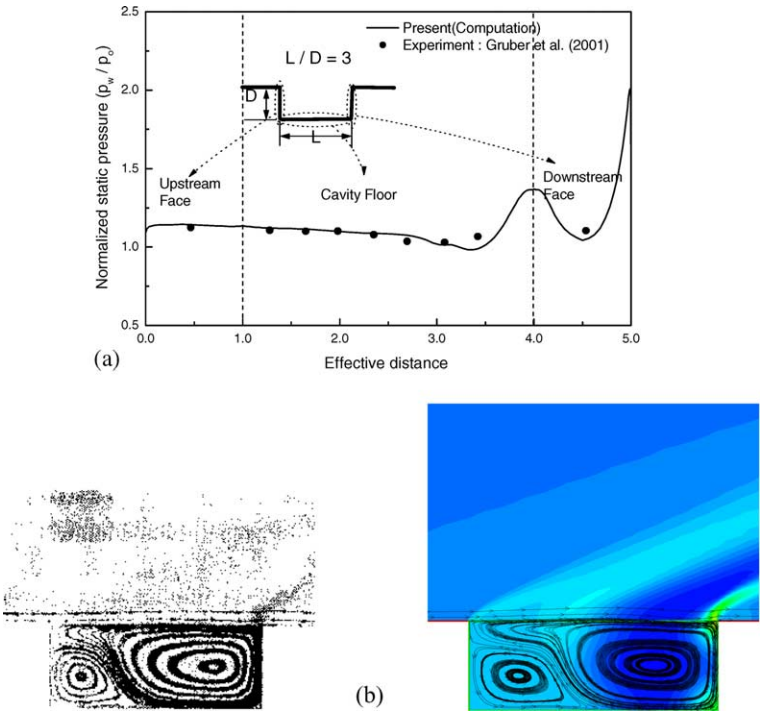

Fig. 4. Computational results for $L/D = 3$. (a) Wall static pressure distribution, (b) streamline and pressure contour (left: Gruber's computational visualization, right: present results).

tion of free stream Mach number of 3.75, total pressure of 1.2 MPa, and total temperature of 299 K. A slot nozzle is convergent sonic throat at the exit. Nozzle width is 1.0 mm while nitrogen gas is injected with total pressure of $p_j = 10.29p_\infty$. The grid system of 141×101 is plotted in Fig. 3(b). In order to see the effects of grid resolution, the static pressure distributions along the wall are presented in Fig. 3(c). It is evident that the grid system of 141×101 is good enough.

In Fig. 3(d), the surface pressure is plotted and compared with the experimental data by Aso et al. as well as other numerical results by Rizzetta [20] and Chenault and Beran [21]. While the current results are reasonable with other numerical results, there is still some discrepancy compared with experimental data. It should be noted that the experimental results do not show a sharp pressure peak just upstream of the slot leading edge. Furthermore, the measured pressure level at upstream of the interaction region ($x/L = 0.9$) is somewhat higher, which maybe is attributable to sharp leading edge of the slot in experiment, but is unaccountable in computation.

As the second test case, a problem of the cavity flow is considered following Gruber et al. [9] who studied several cavity configurations for an unheated flow of Mach 3. Cavities with depth of 8.9 mm were used for experiment for the conditions of $L/D = 3$, $L/D = 5$ without aft angle, and $L/D = 3$ with the aft angle (θ) of 30°. In addition, initial stagnation temperature ($T_{0,\infty}$) and stagnation pressure ($P_{0,\infty}$) of the free stream are 300 K and 690 kPa, respectively.

Fig. 4 presents the surface pressure distribution along the cavity wall for the case of $L/D = 3$. In the figure, the effective distance comprises the cavity upstream forward face from a separation corner, the cavity floor and the cavity rear face. The present calculation is in good agreement with Gruber's experimental one. Also, the computational image of flow field along the cavity are shown and compared with the present numerical one. Experimentally as well as numerically the vortices are well defined within cavity and both compression and expansion waves are well characterized over the cavity. Similarly, Fig. 5 shows the wall pressure distributions for $L/D = 5$ without aft angle and $L/D = 3$ with the aft angle 30. A good agreement is also observed for the computed and experimental results.

3.2. Numerical results

Based on the above validation, the numerical calculation is then applied to a reactive cavity flow with fuel injection at upstream of the cavity for the conditions given in Table 2 [5]. As schematically shown in Fig. 6, the combustor is equipped with cavity, of which aft

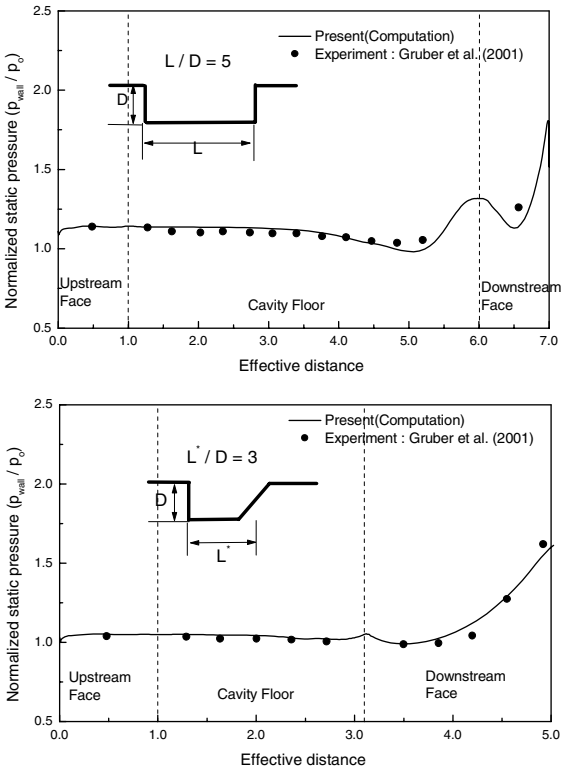

Fig. 5. Wall pressure distribution for $L/D = 5$ and 3 with the aft angle 30°.

Table 2
Computational conditions

Free stream Mach no. of air	$M = 2.5$
Static pressure and static temperature	$P = 1$ atm, $T = 1000$ K
Initial boundary layer thickness	$\delta = 4.5$ mm
Mach no. at injector exit	$M = 1.0$
Stagnation pressure and temperature at injector exit	$P = 7.57$ atm, $T = 600$ K
Size of injector exit	$d = 1$ mm (equivalence ratio $\phi = 0.4$)

angle (θ) is 30° for $L/D = 3$. The model has upstream depth $D_u = 15$ mm. While a no-slip condition is applied along the wall surface, a symmetric condition is imposed on the upper boundary. At the outflow, all the physical variables are extrapolated from the internal cells due to the supersonic flow.

For the basic comparison with other results, the reactive flow field without cavity is solved with hydrogen injected perpendicular to the supersonic freestream. Fig. 7 shows the contours of Mach number, pressure, and temperature. A separation shock, bow shock, Mach disk in the injected flow as well as reattachment shock at downstream of the injector can be identified in the figure. The gas temperature contours show that it becomes more than 2000 K in the upstream separation region under the adiabatic wall condition because no heat produced by the exothermic reaction is lost through the wall. The high temperature region is located near the upstream boundary of the jet above the small-scale recirculation rather than at the center region of the small-scale recirculation. The vicinity of the wall near the small recirculation as well as the downstream region of the injector is filled with unburned fuel gases injected through the injector. The temperature in that region is lower than the injected gas temperature because of under-expansion effects of the injected gas.

The computed results for an inclined cavity are shown in Fig. 8. The bow shock wave by injected fuel jet is seen to interfere with the boundary layer, thereby generating a separation zone in front of the injector. The recirculation zone at upstream of the injector becomes broader compared with the one without cavity. This may result from the lifting effect of the high temperature gas mixture due to the vortices residing in the cavity. The injected gas flows turning after penetrate more into the main stream than that without cavity. The reaction in the cavity acts to expand the gas, causing the shear layer to rise slightly. The strong trailing edge shock wave is also created as the shear layer reattaches at the angled back wall. In Fig. 8(a) the injected jet is seen to span over the cavity until it reaches to the trailing edge of the cavity. Therefore, it can be an open cavity flow. Due to interaction with geometrical configuration, the shear layer over the cavity vertically spreads more broadly compared with the case without cavity. While traveling over the cavity, the injected jet interacts with the strong trailing edge shockwave, which might play an important role in chemical reaction. Furthermore, since the trailing oblique shock wave increases pressure and temperature of the mixture, a shock-induced chemical reaction takes place. It is usually known that a jet interaction with oblique shock wave results in an enhancement in the molecular mixing between supersonic air and jet fuel [22]. The vortices generated by interaction between a shock wave and a shear layer, have immediate influence on the mixing enhancement in supersonic flows, which then results in increasing combustion efficiency. The trailing edge shock is therefore expected to deviate flow direction behind it over the trailing edge of the cavity, thereby, increasing the mixing, the static pressure, the static temperature, and finally the reaction rate.

Figs. 9 and 10 plot a distribution of H_2, OH and H_2O for the case with/without cavity. In case of without cavity, the OH species are primarily produced in the hot separation region upstream of the jet exit and behind the bow shock and convected down stream with shear layer. However, the OH mass fraction decreases as the gas expands around the injected jet and the local mixture temperature falls. It is evident from these results that

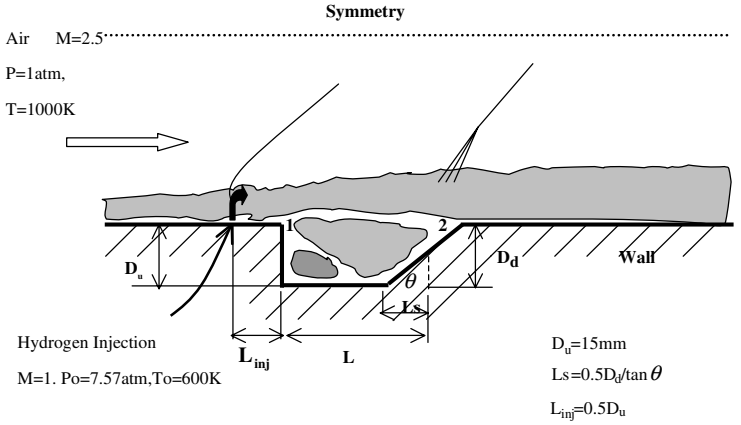

1: leading edge of cavity

2: trailing edge of cavity

θ : aft wall angle

D_u: Upstream depth

D_d: Downstream depth

Fig. 6. Computational geometry and conditions.

improved injection schemes for better flame-holding would be required for practical application in supersonic combustors. In flows around two-dimensional cavities, the boundary layer separate from the upstream lip and reattaches downstream. As the boundary layer separates from the leading edge of the cavity, a free shear layer forms. Depending upon the pressure inside the cavity the shear layer deflects upwards or downwards producing compression or expansion wave consequently. Hydrogen gas is seen to penetrate deeper into the vertical direction for the case with cavity so that the recirculation zone in front of the injector also becomes larger. The gas mixture creates a recirculation region inside the cavity with a hot pool of radicals which will reduce the introduction time, such that autoignition of fuel/air mixture can be obtained. If appropriately considered, a cavity can be an effective tool to improve combustion efficiency as well as flame-holder. According to Figs. 9(b) and (c) and 10(b) and (c), species of OH and H_2O are found even in recirculation zone at upstream of the injector, which means that therein also occurs a chemical reaction. Therefore, the cavity provides a stable pool of hot reaction products. The OH species are primarily produced in the hot separation region upstream of the jet exit and behind the bow shock and convected downstream with the shear-layer. In general, the flame zone is found to be much broader along the downstream for the case with cavity. In Fig. 10(b), the OH mass fraction decreases a bit at midway in front of the trailing edge shock, and then increases at further downstream so that the trailing edge shock is seen to enhance the reaction, thereby making the flame zone behind it broader. As discussed previously, the flame has lifted above the shear layer that separates the cavity fluid from the mainstream. Thus, much of the heat being released by the flow with the cavity is contact with the fuel–air mixture in the mainstream. The lower portion of the mainstream fuel has been reacted in the opening of the cavity, but in the existence of any strong shocks to air in turning the flow and hence spreading the flame, the reaction rate is quite fast and eventually begins to enhance in the rapidly the combustion.

A minimum total pressure loss as well as maximum efficiencies of mixing and combustion should be considered for the optimization of an overall combustor performance with the cavity configuration. Now in order to discuss its performance, the mixing and combustion efficiencies, and stagnation pressure loss are considered in this study. The mixing efficiency is defined in the manner described;

$$\eta_m = \frac{\int \alpha_R \rho u \, dA}{\int \alpha \rho u \, dA}, \quad \alpha_R = \begin{cases} \alpha & \alpha \leqslant \alpha_S \\ \alpha\left(\frac{1-\alpha}{1-\alpha_S}\right) & \alpha > \alpha_S \end{cases}, \tag{22}$$

where, α: fuel mass fraction, α_S: stoichiometric fuel mass fraction, α_R: mass fraction of least available reactant.

The combustion efficiency is a measure of the degree of the completeness of combustion, and defined as;

$$\eta_C = \frac{\dot{m}_{fuel,in} - \dot{m}_{fuel,x}}{\dot{m}_{fuel,in}} \tag{23}$$

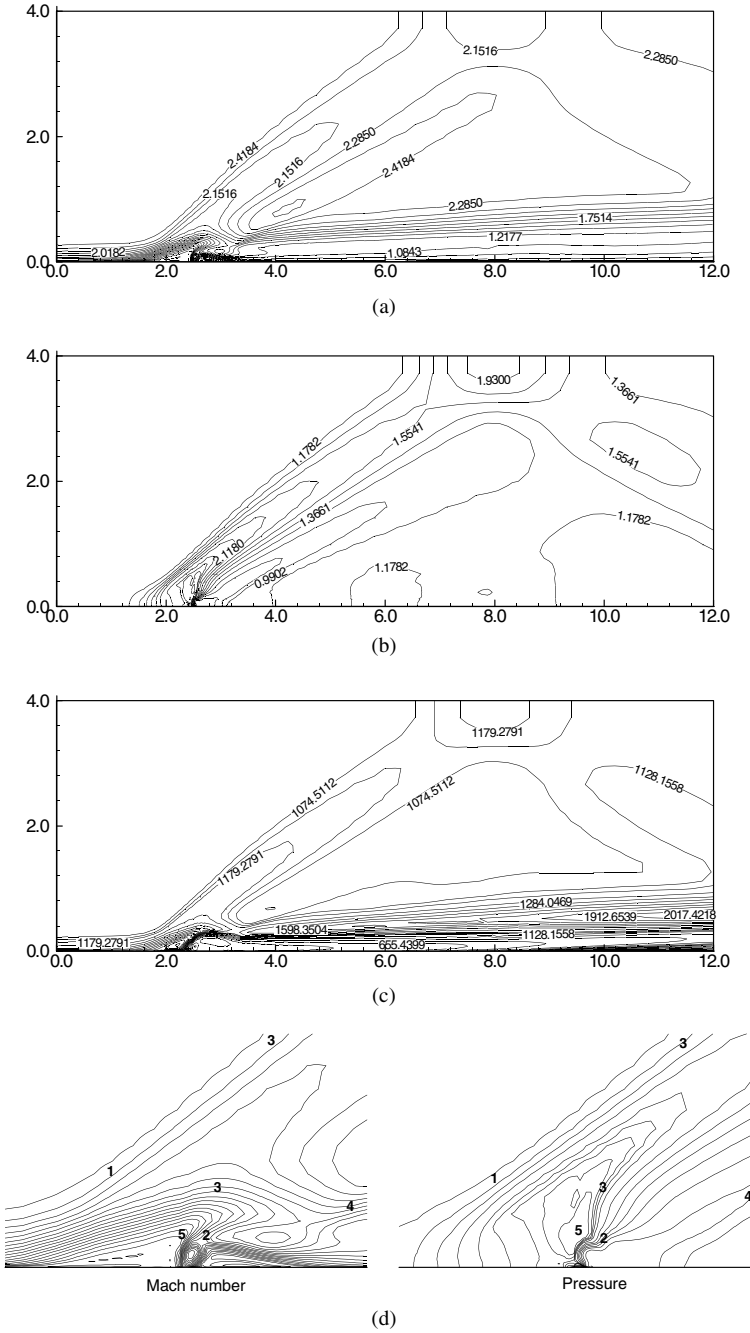

Fig. 7. Computational results for the case without cavity. (a) Mach number contour, (b) pressure contour (p/p_∞), (c) temperature contour (K), (d) Mach number and pressure contour near injector (1: Separation shock, 2: Mach disk, 3: Bow shock, 4: Reattachment shock, 5: Barrel shock).

where $\dot{m}_{\text{fuel},x}$ is local fuel mass flow rate.Also, total pressure loss is

$$\eta_{\text{loss}} = 1 - \frac{\int P_{\text{t}} \rho u \, \mathrm{d}A}{\int P_{\text{t,ref}} \rho u \, \mathrm{d}A} \tag{24}$$

The total pressure is reduced by viscous forces in boundary layer, flow separation, shock wave, fuel-air mixing, and combustion.

First of all, the effect of a cavity on mixing and combustion efficiencies is plotted in Fig. 11. When the

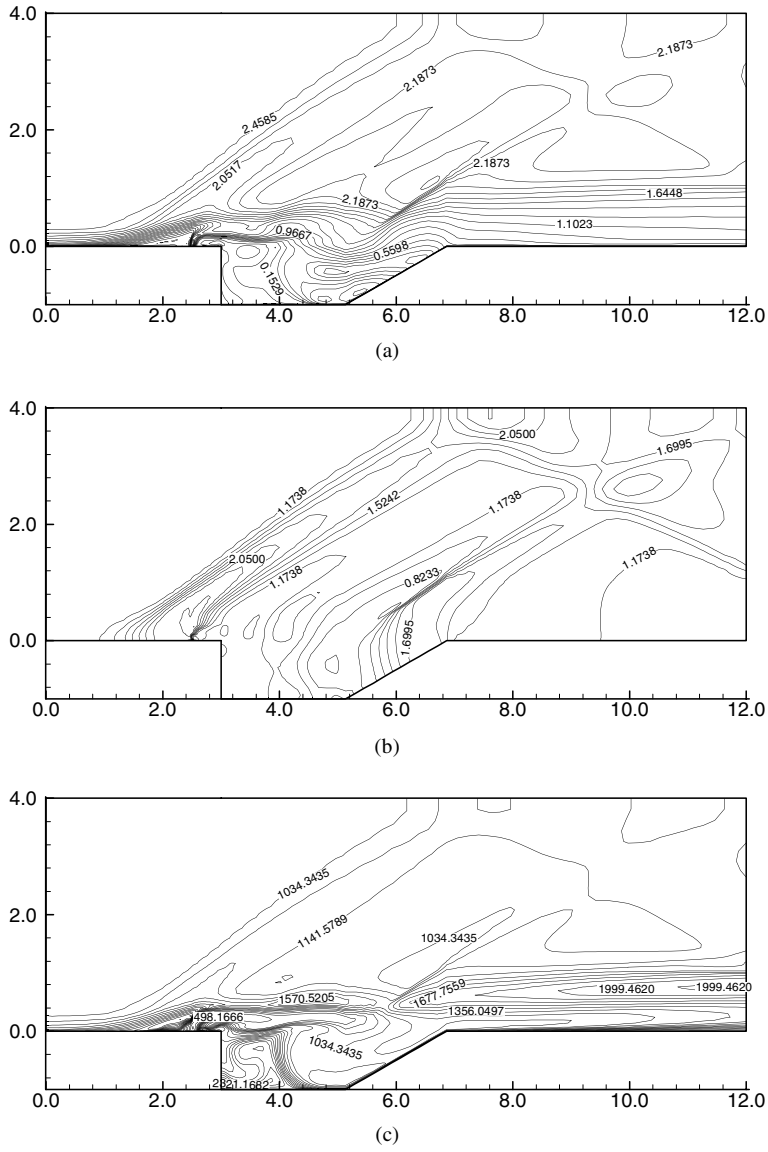

Fig. 8. Computational results for the case with cavity. (a) Mach number contour, (b) pressure contour (p/p_∞), (c) temperature contour (K).

cavity is installed, it is observed in the figure that the combustion as well as mixing efficiency is greatly enhanced, since the mass and thermal transport phenomena are much improved along the shear layer as well as in the cavity. The combustion efficiency is directly related to the total length required for the combustor. The reason is that the higher the combustion efficiency, the shorter the length of combustor becomes.

The cavity shape has to be derived from flow stabilization and flame holding requirements. While the cavity depth can be determined according to the required residence time which provides ignition, the length has to be chosen to sustain a stable vortex inside the cavity. For the cavity effect, we have to analyze the reactive flow field of different cavity geometries; aft wall angle, offset ratio (D_u/D_d), and length L/D.

In Fig. 12, the effects of aft wall angle and offset ratio (D_u/D_d) of upper to downstream depth of the cavity on the vortices are examined. Usually inside the cavity, a couple of vortices are generated, in which the flow velocity is smaller compared with the free stream velocity above it. This induces enough time for the injected fuel and free stream air reside in the cavity to be mixed and then ignited. It is, therefore, evident that the existence of

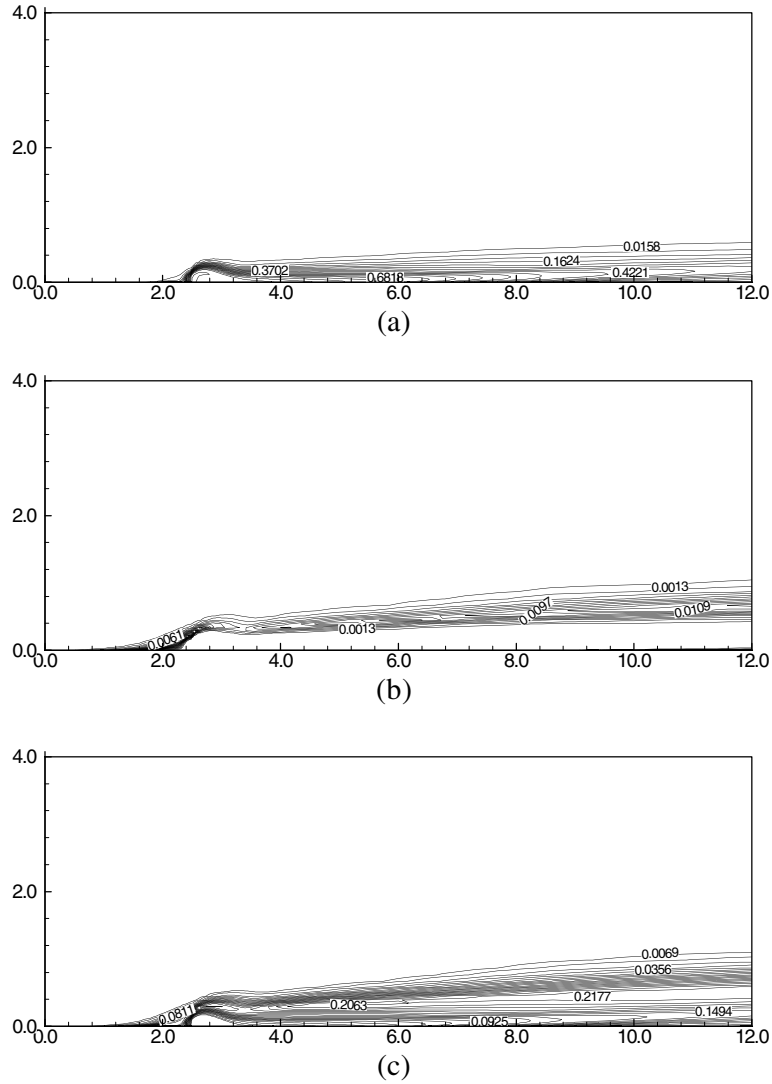

Fig. 9. Computational results for the case without cavity. (a) Mass fraction for H_2, (b) mass fraction for OH, (c) mass fraction H_2O.

the reaction zone in the cavity plays an important role in flame stabilization as shown in the Fig. 8. For an angle of 15°, there are one strong and other minor vortices in the cavity. However, as the aft wall angle increases, the strength of strong vortex becomes weaker, while the minor vortex renders stronger. As the offset ratio increases, the right-hand side vortexes get stronger. These variations in vortex behavior in the cavity may affect the reaction flow field so that their effects are to be more discussed in the below.

Fig. 13 represents the effects of the aft wall angle on the combustion efficiency and total pressure loss. Generally, as the aft wall angle increases, the combustion efficiency increases while the total pressure loss increases. This results from the fact that the strength of the trailing edge shock becomes stronger for higher aft wall angle. Therefore, the combustion efficiency is enhanced while the total pressure, which can be converted to pressure thrust of the vehicle, decreases higher behind the trailing shock.

Fig. 14 illustrates the effects of the offset ratio (D_u/D_d) on the combustion efficiency and total pressure loss. Usually, a part of the injected gas impinges against aft wall, contributing to a formation of trailing edge shock above it, whereas the other part of injected gas flows into the cavity, which reinforces the recirculation zone inside the cavity and then a remaining part of injected gas flows to downstream passing over the trailing edge. The trailing edge shock formation and viscous friction regarding the flows over the trailing edge must

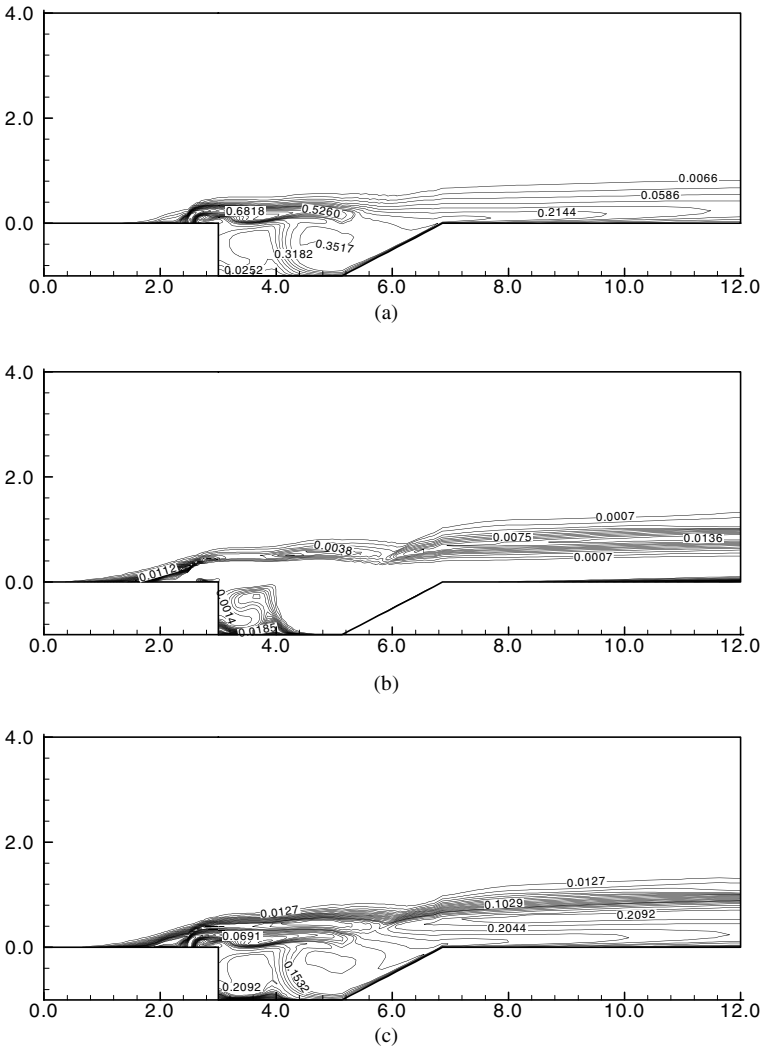

Fig. 10. Computational results for the case with cavity. (a) Mass fraction for H_2, (b) mass fraction for OH, (c) mass fraction H_2O.

accompany the higher total pressure loss. In Fig. 14, as the offset ratio increases, the combustion efficiency is reduced while the total pressure loss decreases. For higher offset ratio, geometrically, the height of trailing edge is lower than that of upstream edge so that the injected gas is more expanded. This would lead to a reduction in gas temperature so that the chemical reaction slowly occurs. Simultaneously, the strength of the trailing edge shock is weaker, which results in smaller total pressure loss. One interesting point in the figure is a comparison between the case without cavity and one for $D_u/D_d = 1.5$. It shows that the fuel injection without cavity yields relatively poor combustion efficiency with even higher total pressure loss. A more total pressure loss for the non-cavity case is due to stronger viscous friction along the wall compared with the case with cavity. For the case with cavity, the reaction is lesser up to the cavity trailing edge ($x/D = 6.5$) because of geometrical gas expansion so that the combustion efficiency is also lower than for the non-cavity case as shown in the figure. However, thereafter, since the flammable gases are ejected from the cavity that plays a role of hot pool, and the fuel lean gases comprises enough radicals, the chemical reaction increases for the case with cavity, whereas fuel is still rich along downstream for the non-cavity. Consequently, based on this comparison, a use of cavity is much preferred.

In Fig. 15, the effect of cavity length is sought for $L/D = 2, 3$, and 4. As the cavity length increases, the total pressure loss does too. However, the combustion efficiency is the highest for medium cavity length of $L/D = 3$. In other words, a very short cavity length yields a poor combustion while too long cavity length results in a higher total pressure loss. Consequently, a

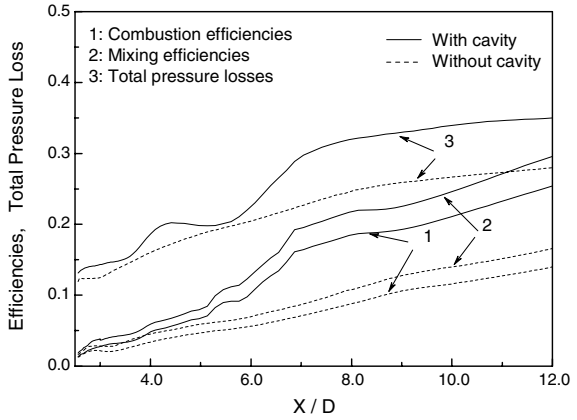

Fig. 11. Combustion and mixing efficiencies for the combustor with/without cavity.

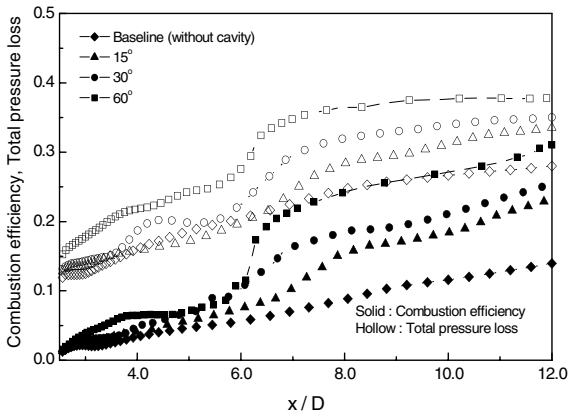

Fig. 13. Combustion efficiency and total pressure loss for various aft wall angles.

use of appropriate length of cavity is preferred to attain best combustion efficiency with moderate total pressure loss.

Fig. 16 shows the change of the location of the injector; $L_{inj} = D_u$, $L_{inj} = 1/2D_u$, and $L_{inj} = 1/4D_u$. If the injector is relatively far from the leading edge of the cavity, the cavity has formed small vortices because the mixture entering the cavity was not enough. For the reason, the shear layer goes down to the cavity opening. Also the cavity has weak trailing edge shock. On the other hand, if the injector is relatively closer, injected fuel does not deeply penetrate in the free stream due to the flow turning by the cavity configuration so that the plenty of the mixture enters into a cavity. Therefore, the reactive region in the cavity can not transfer much released heat to the shear layer due to the formation of

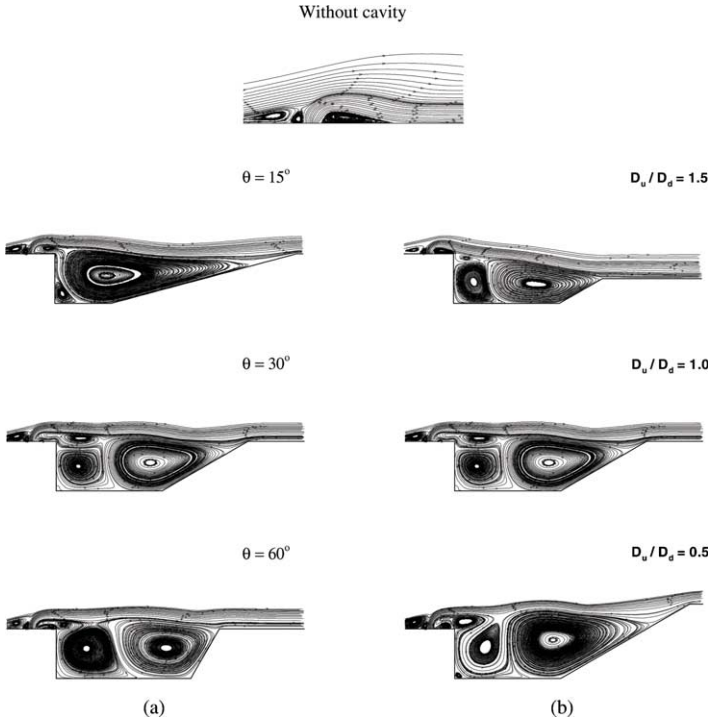

Fig. 12. Streamlines for various cavity configurations. (a) Angle variations in case of $D_u/D_d = 1.0$. (b) Offset ratio variations in case of $\theta = 30°$.

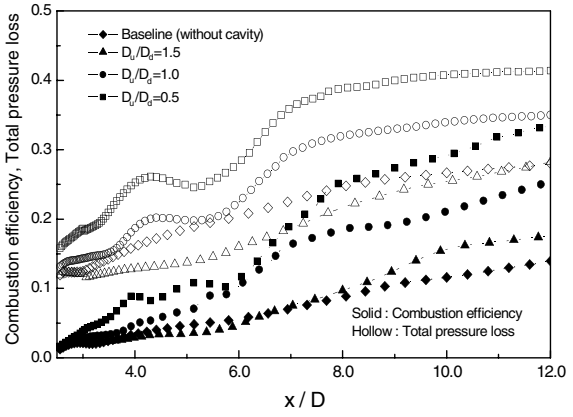

Fig. 14. Combustion efficiency and total pressure loss for various offset ratios (D_u/D_d).

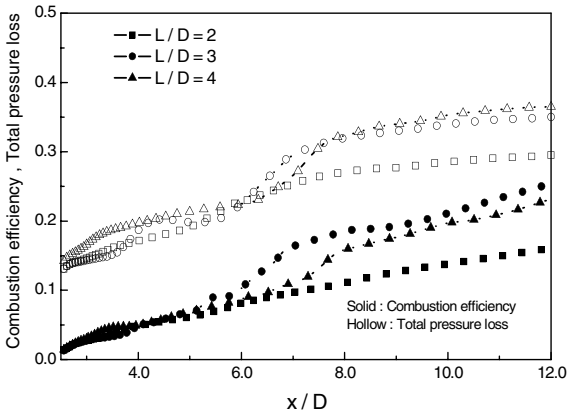

Fig. 15. Combustion efficiency and total pressure loss for various cavity lengths.

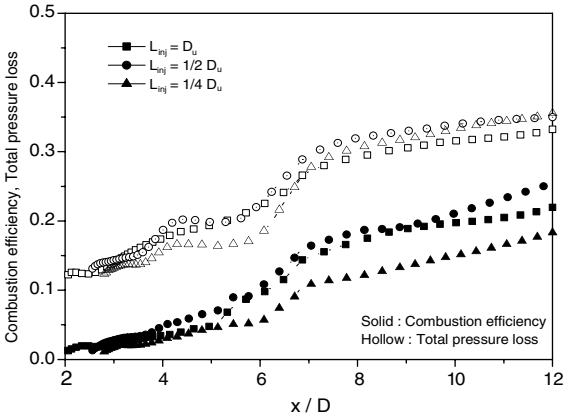

Fig. 16. Combustion efficiency and total pressure loss for the change of the location of the injector.

recirculation region with low temperature. These result in low combustion efficiency.

4. Conclusions

In this study, the effects of the cavity on the hydrogen injection into the supersonic air flow have been investigated. Usually, the cavity was found to increase both the total pressure loss and the temperature of the combustor while enhancing the combustion of fuel and oxidizer. By varying the aft wall angle, the offset ratio of upstream to downstream depth and the cavity length the following main results were found.

(1) When the aft wall angle of cavity increases, the combustion efficiency is improved, but total pressure loss increased. In these regards, the trailing edge shock over the cavity must play an important role.
(2) When the offset ratio of upper to downstream depth of the cavity increases, the combustion efficiency as well as the total pressure loss decreases. For higher offset ratio, geometrically the injected gas has expanded more, resulting in reduction in gas temperature so that the chemical reaction has been retarded. Based on comparison with the case without cavity, a use of cavity is much preferred.
(3) When the cavity length is changed, the combustion efficiency is the highest for an appropriate cavity length with moderate total pressure loss. Consequently, a best choice for the length of cavity exists regarding the combustion efficiency and total pressure loss.

Acknowledgements

The financial assistance by the Center for Electro-Optics at KAIST is gratefully acknowledged.

References

[1] H.A. Berman, J.D. Anderson Jr., J.P. Drummond, Supersonic flow over a rearward facing step with transverse nonreacting hydrogen injection, AIAA J. 21 (1983) 1707–1713.
[2] A.S. Roudakov, Y. Schikhmann, V. Semenov, Ph. Novelli, O. Fourt, Flight testing an axisymmetric scramjet—Russian recent advances, in: 44th IFA Congress, IFA Paper 93-S.4.485, 1993.
[3] Ben-Yakar Adela, Natan Benveniste, Gany Alon, Investigation of a solid fuel scramjet combustion, J. Propul. Power 14 (1) (1998) 447–455.
[4] Adela Ben-Yakar, R.K. Hanson, Cavity flameholders for ignition and flame stabilization in scramjets: review and experimental study, AIAA-98-3122, 1998.

[5] X. Zhang, Compressible cavity flow of oscillation due to shear layer instabilities and pressure feedback, AIAA J. 33 (8) (1995) 1404–1411.
[6] X. Zhang, A. Rona, J.A. Edwards, The effect of trailing edge geometry on cavity flow oscillation driven by a supersonic shear layer, Aeronaut. J. (1998) 129–136.
[7] R.L. Sarno, M.E. Franke, Supression of flow-induced pressure oscillations in cavities, J. Aircraft 31 (1) (1994) 96–99.
[8] R.A. Baurle, M.R. Gruber, A study of recessed cavity flowfields for supersonic combustion applications, AIAA-98-0938, 1998.
[9] M.R. Gruber, R.A. Baurle, T. Mathur, K.-Y. Hsu, Fundamental studies of cavity-based flameholder concepts for supersonic combustors, J. Propul. Power 17 (1) (2001) 146–153.
[10] K.-Y. Hsu, L.P. Goss, W.M. Roquemore, Characteristics of a trapped-vortex combustor, J. Propul. Power 14 (1998) 57–65.
[11] K. Yu, K.J. Wilson, K.C. Schadow, Effect of flame-holding cavities on supersonic combustion performance, AIAA-99-2638, 1999.
[12] S. Chapman, T.G. Cowling, The Mathematical Theory of Non-Uniform Gases, Cambridge, 1970.
[13] C.R. Wilke, A viscosity equation for gas mixtures, J. Chem. Phys. 18 (1950) 517–519.
[14] B.S. Baldwin, H. Lomax, Thin layer approximation and algebraic model for separated turbulent flow, AIAA-78-257, 1978.
[15] S. Gordon, B.J. Mcbride, Computer program for calculation of complex chemical equilibrium compositions, rocket performance, incident and reflected shocks, and Chapman-Jougueet detonations, NASA SP-273, 1971.
[16] J.S. Shuen, M.S. Liou, B. van Leer, Inviscid flux-splitting algorithms for real gases with non-equilibrium chemistry, J. Comput. Phys. 90 (1990) 371–395.
[17] J.S. Evans, C.J. Schexnayder Jr., Influence of chemical kinetics and unmixedness on burning in supersonic hydrogen flames, AIAA J. 18 (1980) 188–193.
[18] J.S. Shuen, Upwind differencing and LU factorization for chemical non-equilibrium Navier–Stokes equations, J. Comput. Phys. 33 (1992) 233–250.
[19] S. Aso et al., Experimental study on mixing phenomena in supersonic flows with slot injection, AIAA-91-0016, 1991.
[20] D.P. Rizzetta, Numerical simulation of slot injection into a turbulent supersonic stream, AIAA J. 30 (1992) 2434–2439.
[21] C.F. Chenault, P.S. Beran, k–ε and Reynolds stress turbulence model comparisons for two-dimensional injection flows, AIAA J. 36 (1998) 1401–1412.
[22] Adela Ben-Yakar, Ronald K. Hanson, Supersonic combustion of cross-flow jets and influence of cavity flameholders, AIAA-99-0484, 1999.